Electronic Supplementary Material (ESI) for Journal of Materials Chemistry A.

Supplementary Information for

Solar driven efficient conversion of methane to multicarbon oxygenates†

Guanghui Feng,‡[ab] Yonghui Zhao,‡[a] Cuijie Ma,‡[ac] Wei Chen,*[a] Tong Li,[ab] Xiaoju Zhao,[ab] Guihua Li,[ab] Xiao Dong,[a] Yanfang Song,[a] Wei Wei,*[ac] Yuhan Sun,*[ac]

[a] CAS Key Laboratory of Low-Carbon Conversion Science and Engineering, Shanghai Advanced Research Institute, Chinese Academy of Sciences, Shanghai 201210, P.R. China

[b] University of Chinese Academy of Sciences, Beijing 100049, P.R. China

[c] School of Physical Science and Technology, ShanghaiTech University, Shanghai 201210, P.R. China

‡ These authors have contributed equally.

* E-mail: chenw@sari.ac.cn, weiwei@sari.ac.cn, sunyh@sari.ac.cn

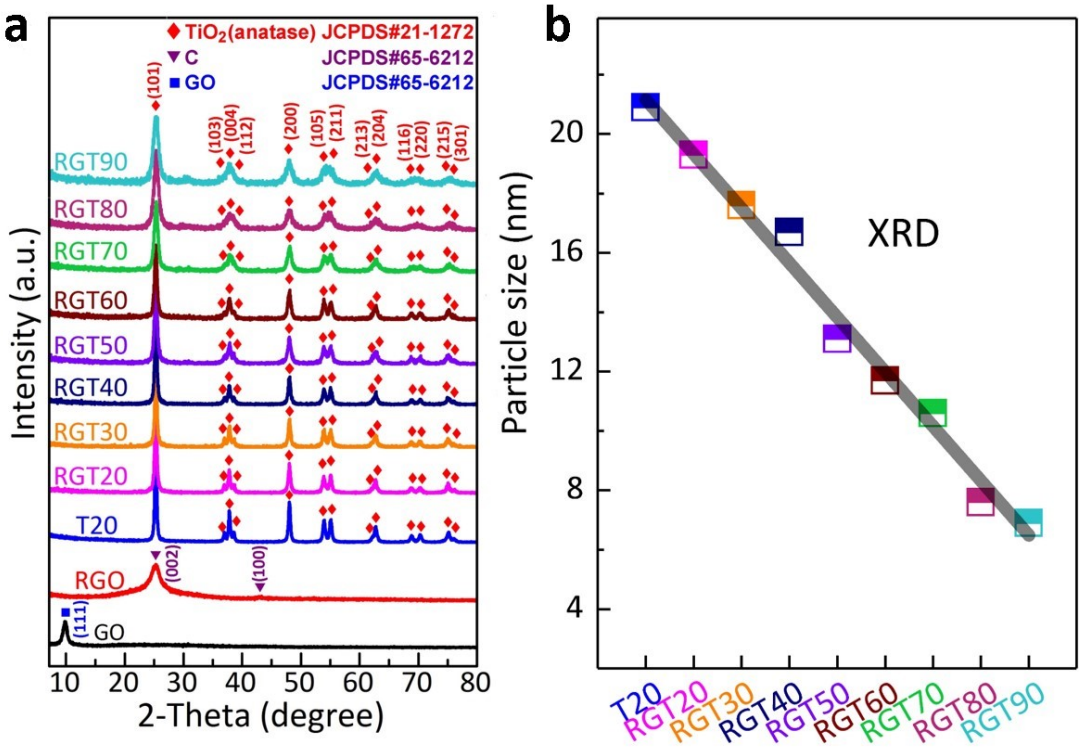

Fig. S1. (a) XRD patterns of GO, RGO, T20 and RGTX in the range of 5°-80°, X=20, 30, 40, 50, 60, 70, 80 and 90, as in Fig. 1b in the main text; (b) Comparison of particle size based on a calculation using the Scherrer equation on account of the TiO_2(200) peak.

The particle size of TiO_2 in the T20 and RGTX samples calculated by using the Scherrer equation differs from that obtained from the TEM size distribution, but the trend of the particle size change is consistent, i.e., the temperature of ultrapure water during hydrolysis of titanium precursors has a large effect on the particle size, and as the temperature of the ultrapure water increases, the water vapor concentration increases and the hydrolysis rate increases, leading to a decrease in the particle size of TiO_2.

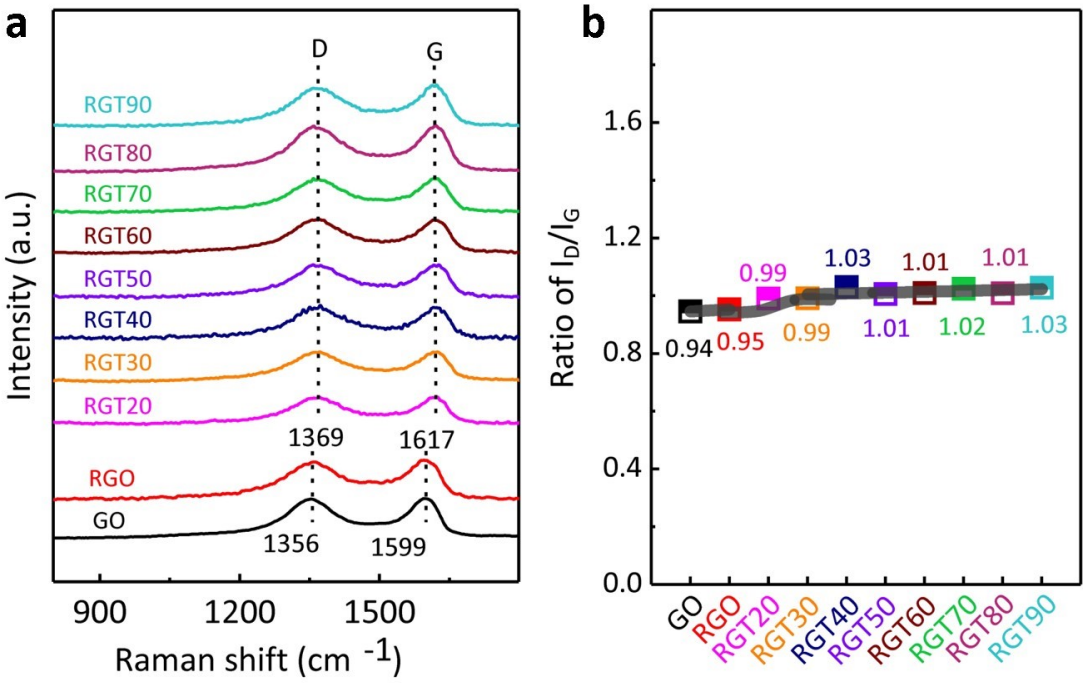

Fig. S2. (a) D bands and G bands in the Raman spectra of the GO, RGO, T20 and RGTX samples; (b) Comparison of the intensity ratio of the D band to the G band (I_D/I_G) over the GO, RGO, T20 and RGTX samples.

Figure S2† shows the peak shift and intensity ratio (I_D/I_G) of the D band and the G band in the Raman spectra of GO, RGO and RGO in the T20 and RGTX samples, indicating that GO is partially reduced to RGO and interacts with TiO_2 particles in the RGTX samples.

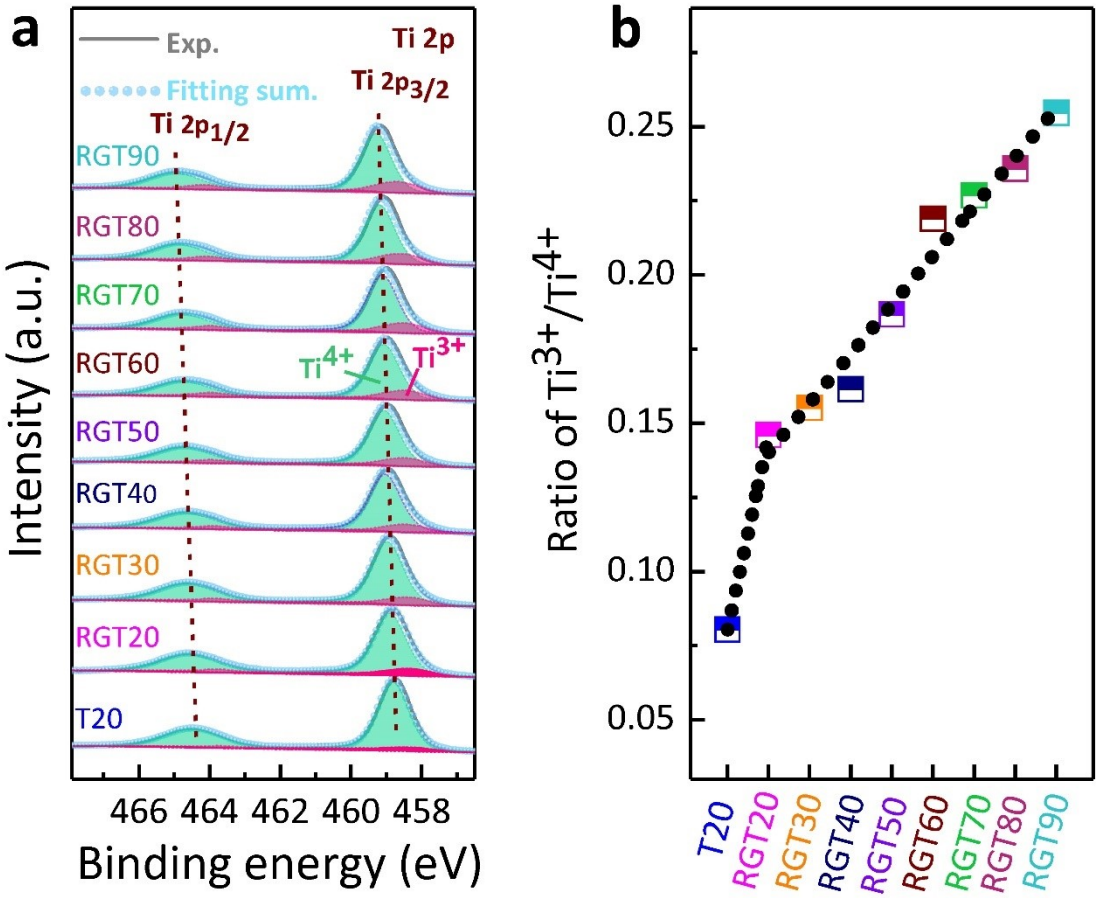

Fig. S3. (a) High-resolution Ti2p XPS spectra of the T20 and RGTX samples; (b) The Ti^{3+}/Ti^{4+} ratio over the T20 and RGTX samples.

The Ti 2p XPS spectra of the T20 and RGTX samples could be fitted with four distinct peaks: Ti^{4+} 2p 3/2, Ti^{4+} 2p 1/2, Ti^{3+} 2p 3/2, and Ti^{3+} 2p 1/2. The Ti^{3+}/Ti^{4+} ratio increased with increasing ultrapure water temperature. Moreover, the concentration of O-vacancies and Ti^{3+} defects determined from the EPR spectrum **(Fig. 1e)** and the fitted data for the Ti^{3+}/Ti^{4+} ratio further indicated that O-vacancies and Ti^{3+} defects can be quantitative. Compared to pristine TiO_2, RGTX presents Ti 2p3/2 and Ti 2p1/2 peaks that are positively shifted to different degrees, which could be ascribed to the high dispersion of small TiO_2 particles and the reduced electron cloud density of Ti caused by the interaction between RGO and TiO_2. The presence of Ti^{3+} species indicates that Ti^{4+} ions obtain electrons from nearby O-vacancies, which indirectly proves the existence of O-vacancies in TiO_2 **(Fig. 1e)**.

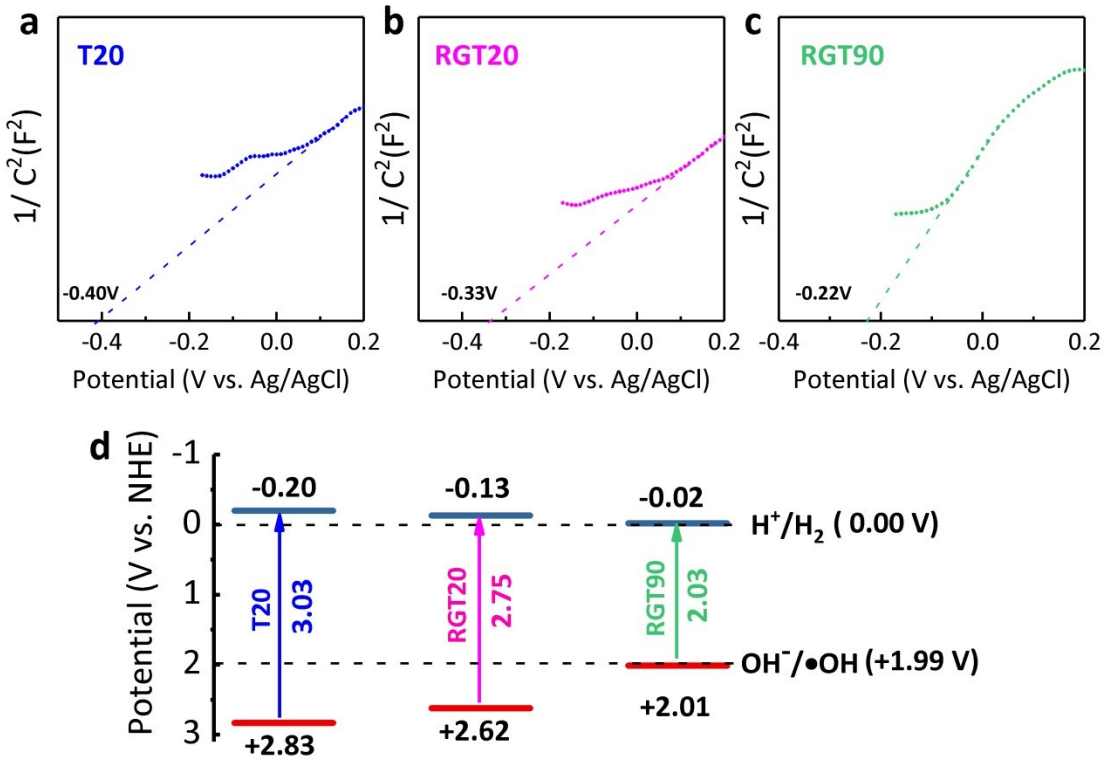

Fig. S4. Mott-Schottky plots of (a) T20, (b) RGT20 and (c) RGT90 and (d) their corresponding energy band structure alignments.

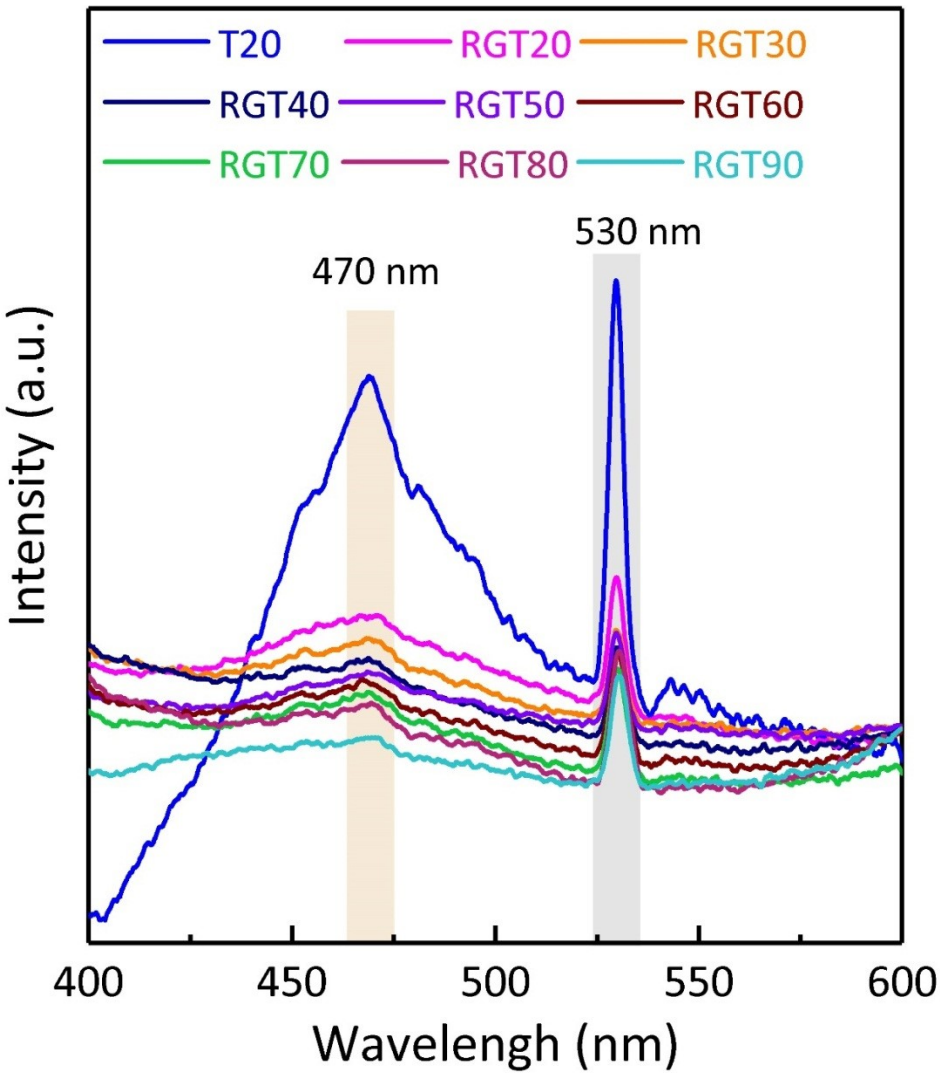

Fig. S5. PL spectra of the T20 and RGTX catalysts.

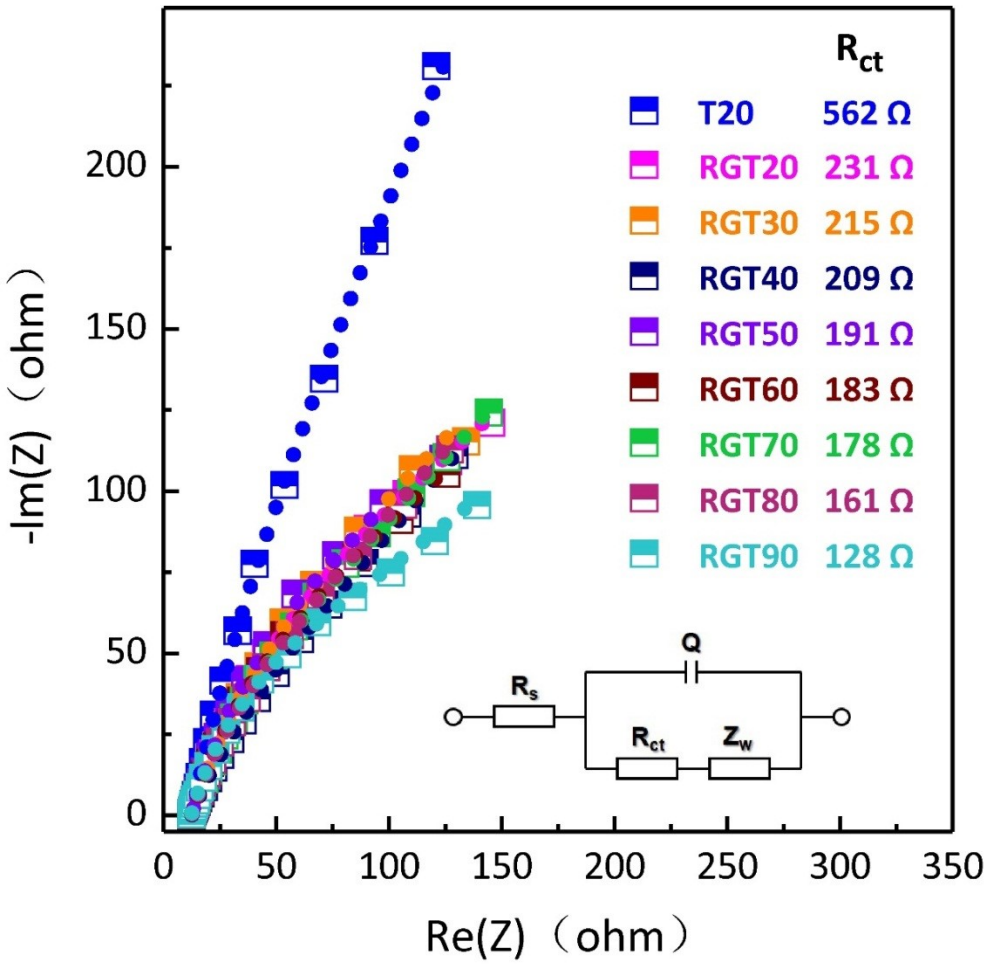

Fig. S6. EIS Nyquist plots of the T20 and RGTX catalysts. The dotted lines indicate the fits to the experimental data (pentagram dots) using the equivalent circuit in the inset. Inset: Equivalent circuit model. (R_s refers to the series resistance, and R_{ct} and Z_w are the charge transfer resistance and the constant phase element, respectively.)

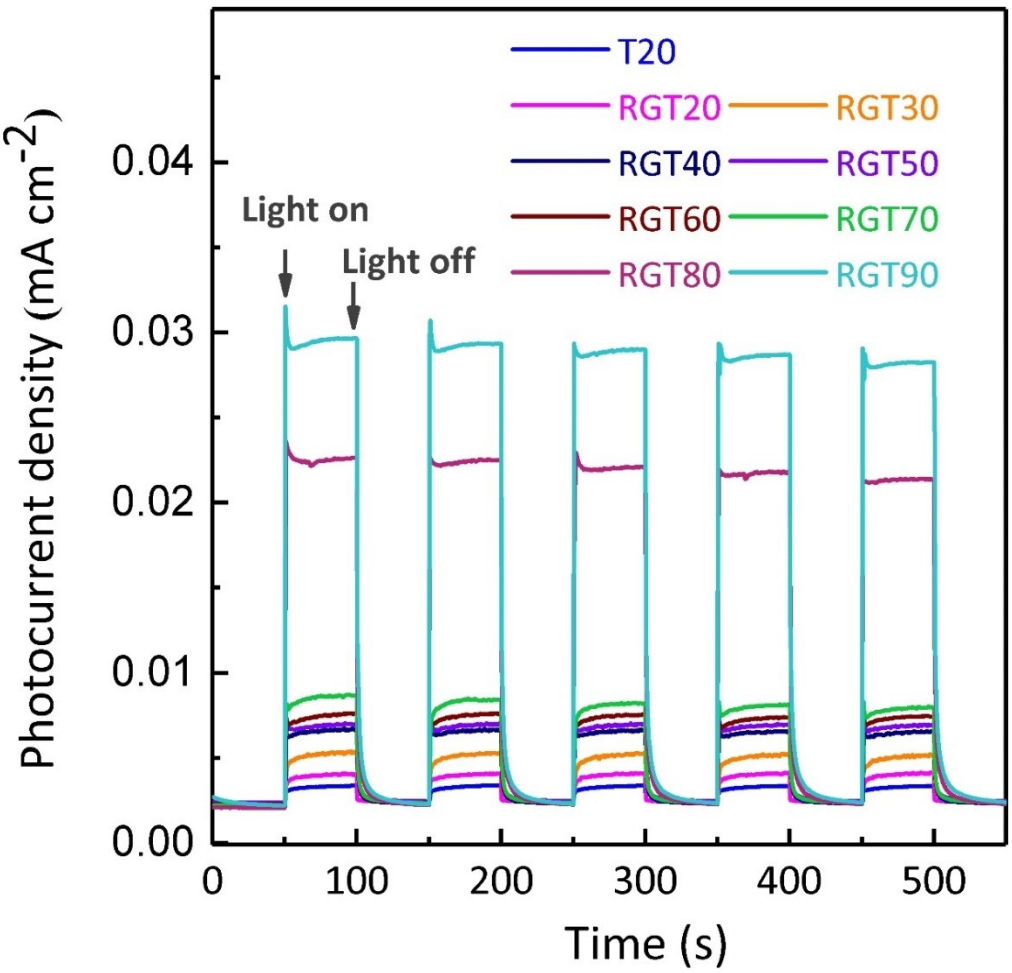

Fig. S7. Transient photocurrent curves of the T20 and RGTX catalysts under simulated solar light Xe lamp irradiation with an air mass (AM) 1.5 filter with a 0 mV bias (vs. Ag/AgCl). The arrows show the times of light on and light off.

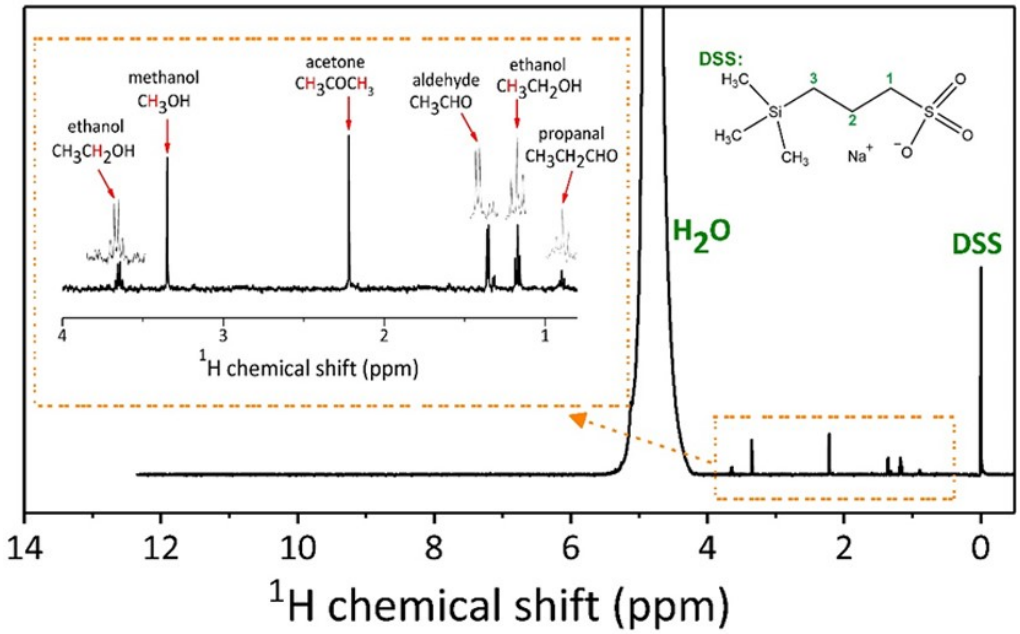

Fig. S8. ^{1}H NMR spectrum of the reaction products from POM with water vapor by the RGT90 catalyst. Reaction conditions: 2 mg of catalyst, the tail gas of the reaction was collected in an ice bath of 2 mL of deionized water, and the reaction was carried out at 60 °C for 5 h at atmospheric pressure CH_4.

By prolonging the reaction time to 5 h and collecting the reaction gas in ultrapure water in an ice-water bath, peaks attributed to methanol, aldehyde, ethanol, propanal and acetone appeared in the HNMR spectrum, further providing clear evidence of the generation of multicarbon oxygenates (**Fig. 2a and b**).

No.	Time min	Peak Name	Peak Type	Area µS*min	Height µS	Amount
1	4.01	Ac	BM *	0.016	0.077	n.a.
2	4.45	HCOO	MB*	0.008	0.042	n.a.
TOTAL:				0.02	0.12	0.00

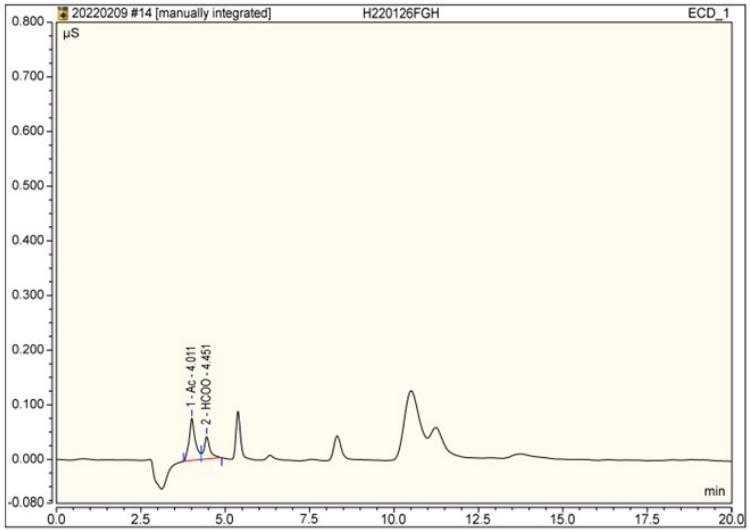

Fig. S9. Ion chromatography curve of the reaction products from POM with water vapor by the RGT90 catalyst. Reaction conditions: 2 mg of catalyst, the tail gas of the reaction was collected in an ice bath of 5 mL of deionized water, and the reaction was carried out at 60 °C for 5 h at atmospheric pressure CH_4.

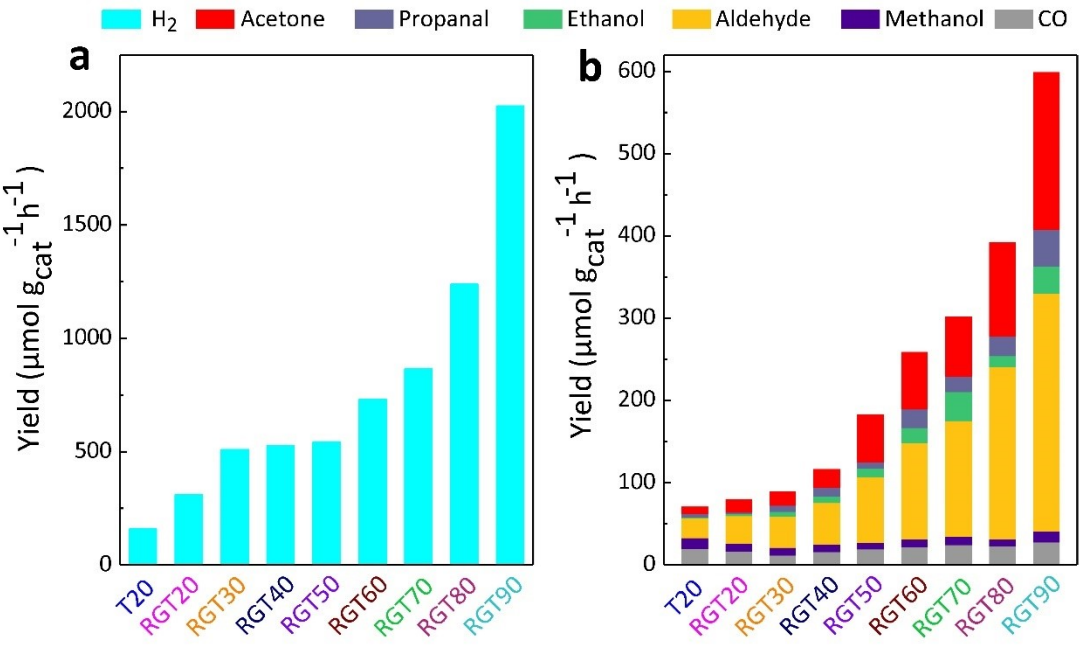

Fig. S10. (a) Yield of H_2 over T20 and RGTX for POM with H_2O under simulated sunlight irradiation; (b) Yield over T20 and RGTX for POM with H_2O under simulated sunlight irradiation. Fig. S8b is the same as Fig. 2b in the main text.

In consideration of charge balance throughout the whole system, we calculated the theoretical yield of the reduced product (H_2) by the total electron gain/loss transfer of the oxidized product (CO, CH_3OH, CH_3CHO, CH_3CH_2OH, CH_3CH_2CHO and CH_3COCH_3).

$$CH_4 - 6e^- \rightarrow CO \qquad \text{eq. (1)}$$

$$CH_4 - 2e^- \rightarrow CH_3OH \qquad \text{eq. (2)}$$

$$2CH_4 - 6e^- \rightarrow CH_3CHO \qquad \text{eq. (3)}$$

$$2CH_4 - 4e^- \rightarrow CH_3CH_2OH \qquad \text{eq. (4)}$$

$$3CH_4 - 8e^- \rightarrow CH_3COCH_3 \qquad \text{eq. (5)}$$

$$3CH_4 - 8e^- \rightarrow CH_3CH_2CHO \qquad \text{eq. (6)}$$

$$2H+ \; 2e^- \rightarrow H_2 \qquad \text{eq. (7)}$$

As displayed in eqs. (1)-(6) above, for the purpose of calculation, we assumed that the yields of CO, CH_3OH, CH_3CHO, CH_3CH_2OH, CH_3CH_2CHO and CH_3COCH_3 were a, b, c, d, e and f, respectively, and the total number of electrons lost in the oxidation products was 6a + 2b + 6c + 4d + 8e + 8f. According to eq. (7), assuming that the theoretical yield of H_2 is g, the total number of electrons gained is 2g. The conservation of electrons gained and

lost, 6a + 2b + 6c + 4d + 8e + 8f = 2g, was used to calculate the theoretical hydrogen yields of T20, RGT20, RGT30, RGT40, RGT50, RGT60, RGT70, RGT80 and RGT90 for photocatalytic methane with water: 158.6 μmol·g_{cat}^{-1}·h^{-1}, 308.6 μmol·g_{cat}^{-1}·h^{-1}, 509.4 μmol·g_{cat}^{-1}·h^{-1}, 526.7 μmol·g_{cat}^{-1}·h^{-1}, 543.8 μmol·g_{cat}^{-1}·h^{-1}, 730.6 μmol·g_{cat}^{-1}·h^{-1},866.3 μmol·g_{cat}^{-1}·h^{-1}, 1237.8 μmol·g_{cat}^{-1}·h^{-1} and 2025.8 μmol·g_{cat}^{-1}·h^{-1}, respectively. This is not much different from the actual measured hydrogen production **(Fig. S10a†)**, so we think that the occurrence of redox reactions in pairs in POM process.

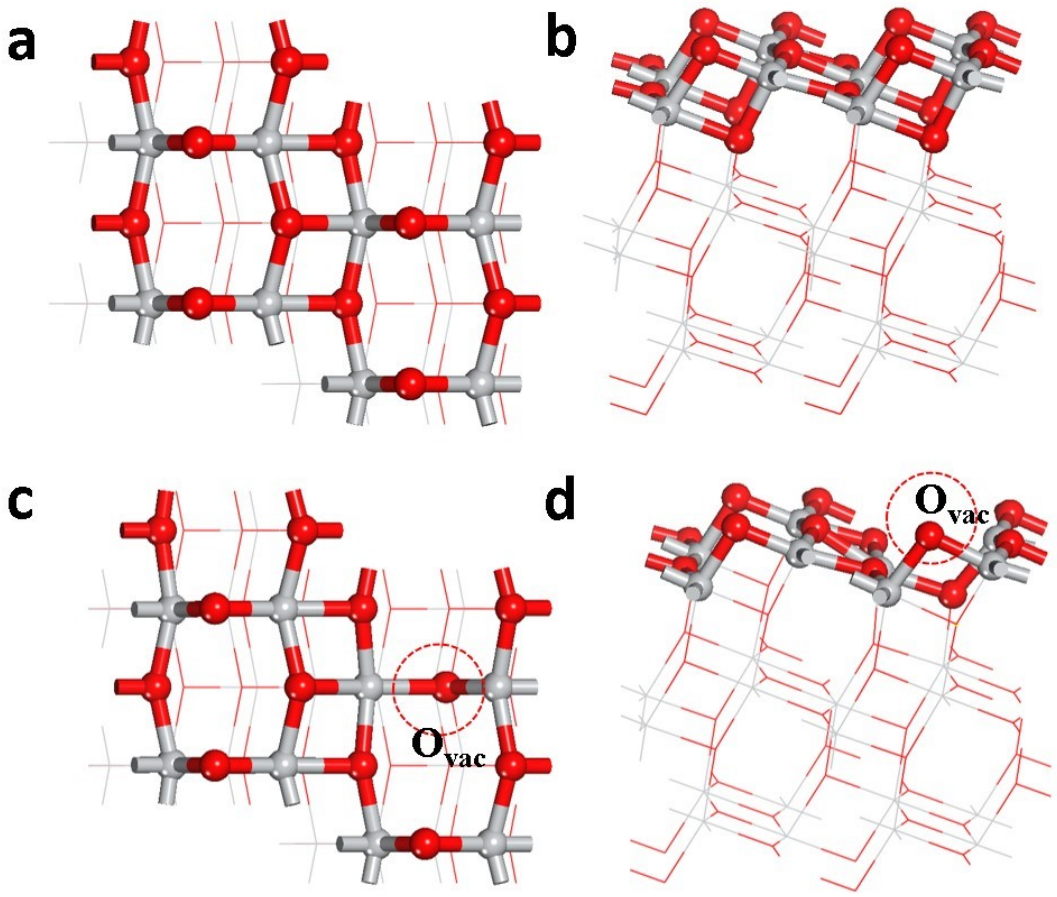

Fig. S11. Top and side views of the 2 × 2 supercell structure of the TiO_2(101) surface (a, b) and O-vacancy/TiO_2(101) surface (c, d). O_{vac} denotes the twofold-coordinate O atom vacancy. (Dark gray: C; light gray: C; red: O; white: H). Figs. S9c and d are the same as Fig. 3b and a in the main text, respectively.

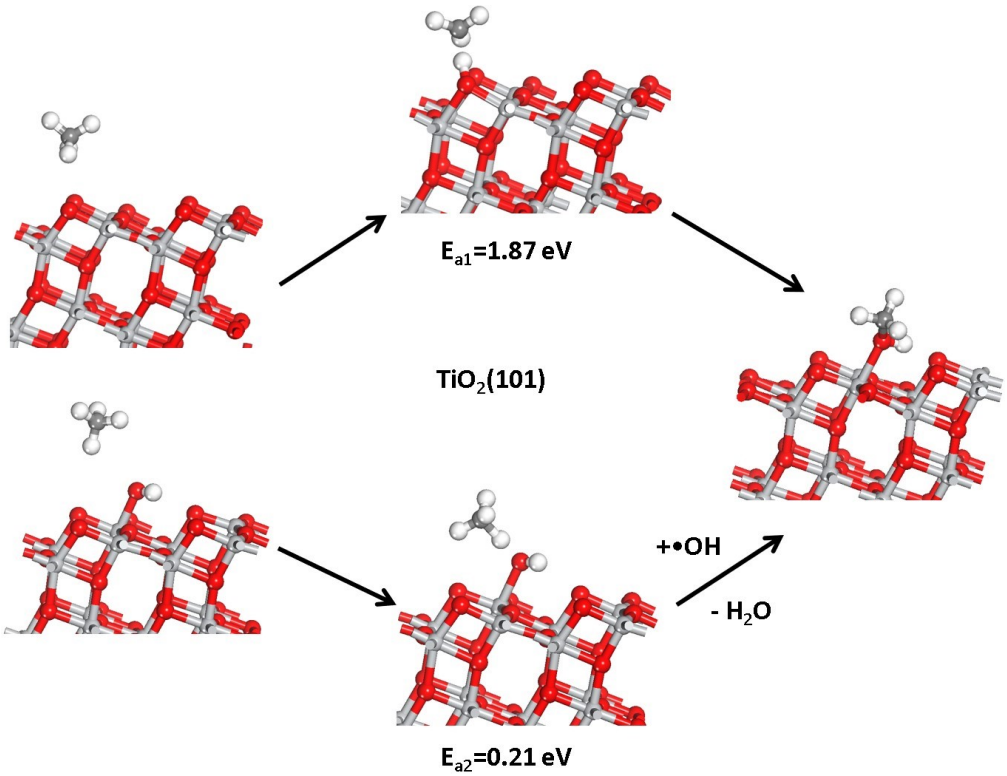

Fig. S12. Two possible pathways for CH_4 dissociation on the TiO_2(101) surface: direct dissociation mechanism (above) and •OH-assisted dissociation mechanism (below). (Dark gray: C; light gray: C; red: O; white: H).

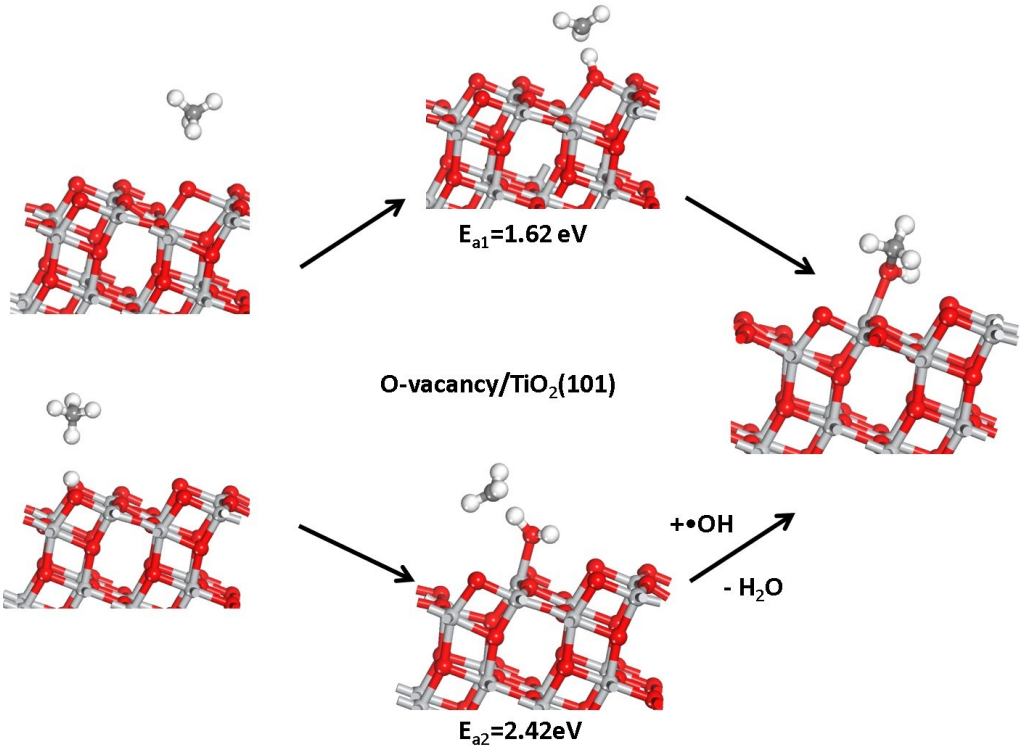

Fig. S13. Two possible pathways for CH_4 dissociation on the O-vacancy/TiO_2(101) surface: direct dissociation mechanism (above) and •OH-assisted dissociation mechanism (below). (Dark gray: C; light gray: C; red: O; white: H).

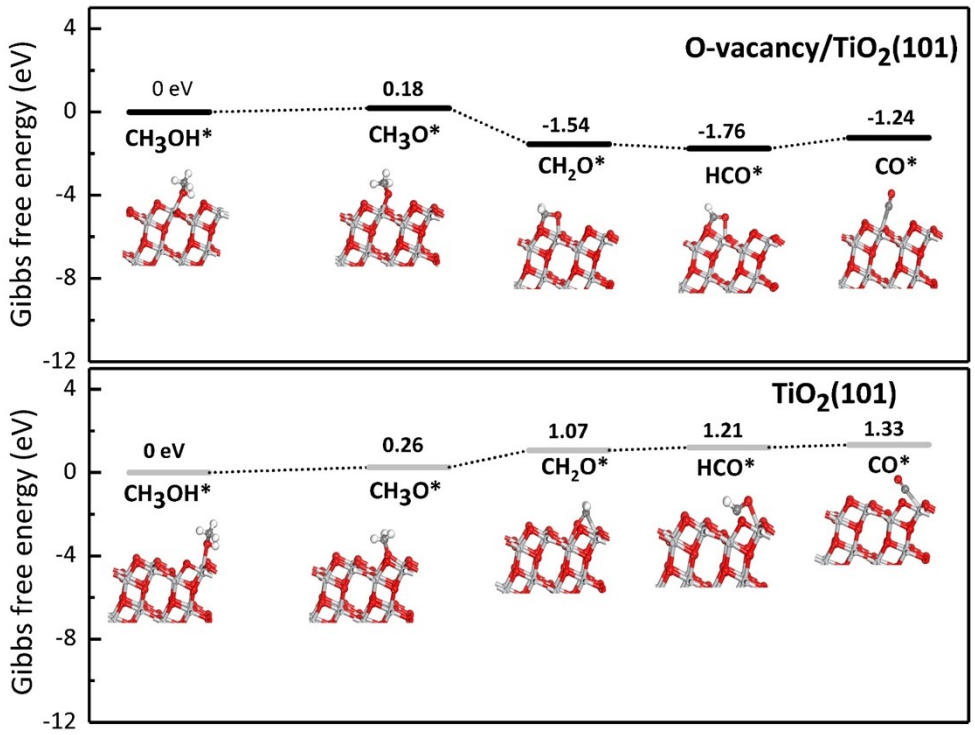

Fig. S14. Free energy diagrams calculated for the pathways of photooxidation of CH_3OH by •OH radicals on TiO_2(101) surfaces (top) and O-vacancy/TiO_2(101) surfaces (bottom). Inset: Optimized structures of reaction intermediates in the pathways (Dark gray: C; light gray: C; red: O; white: H).

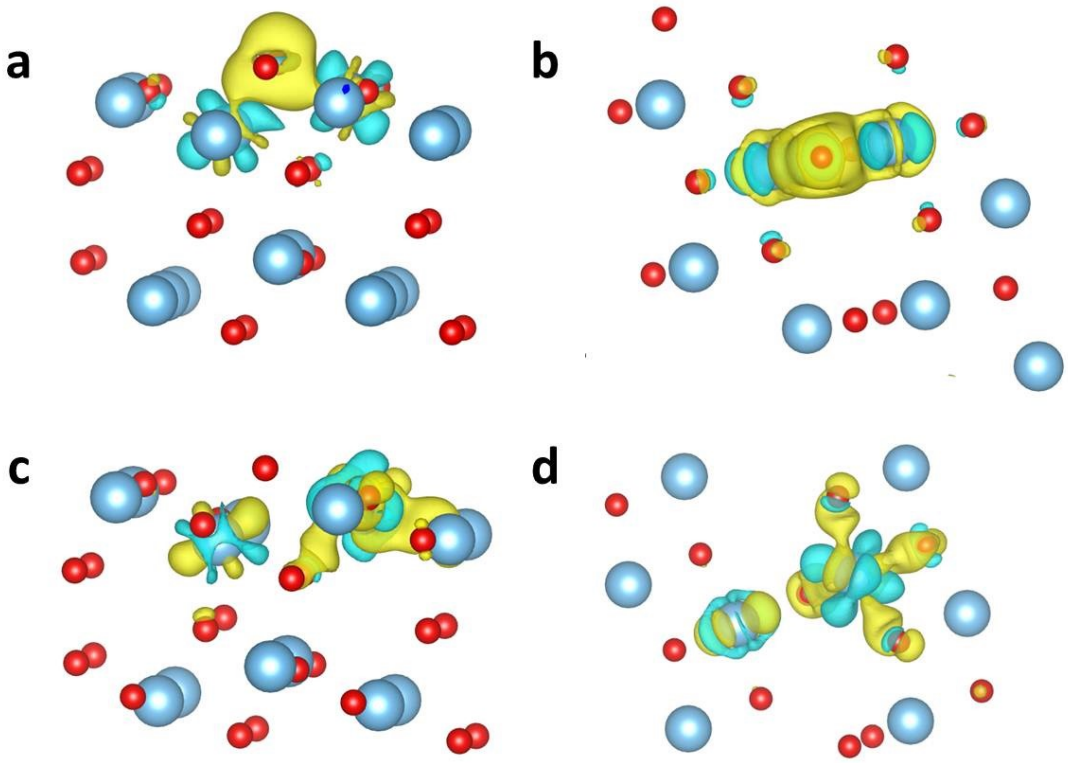

Fig. S15. Side and top views of the difference between charge densities of the perfect TiO_2(101) surfaces (a, b) and O-vacancy/TiO_2(101) surfaces (c, d); the isosurface value is 0.01 e/Å^3. The blue and yellow lobes represent the negative and positive levels of isosurfaces, respectively.

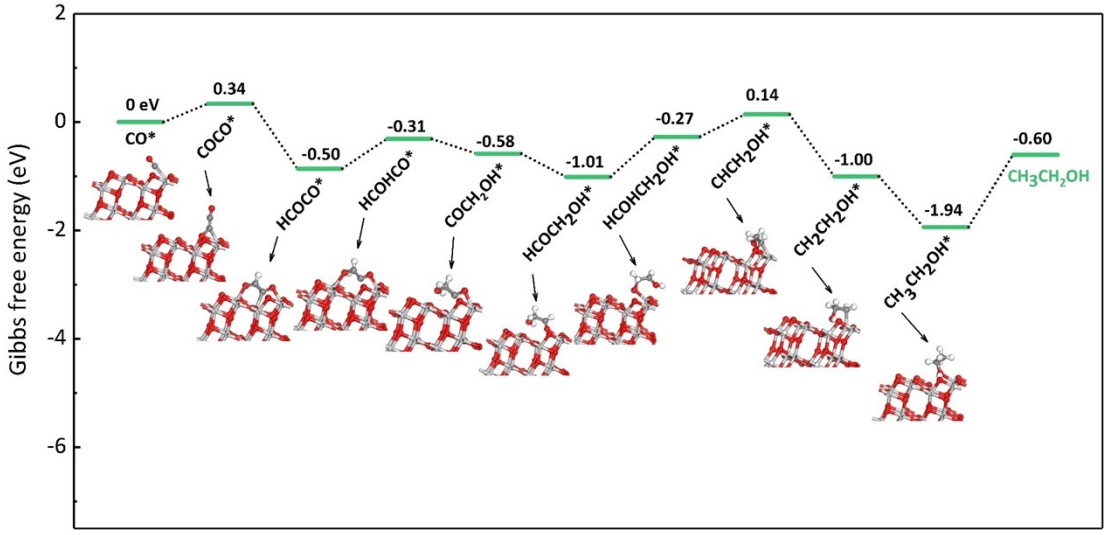

Fig. S16. Free energy diagrams calculated for the pathways CO reduction to CH_3CH_2OH on O-vacancy/TiO_2(101) surfaces. Inset: Optimized structures of the reaction intermediates in the pathways (Dark gray: C; light gray: C; red: O; white: H).

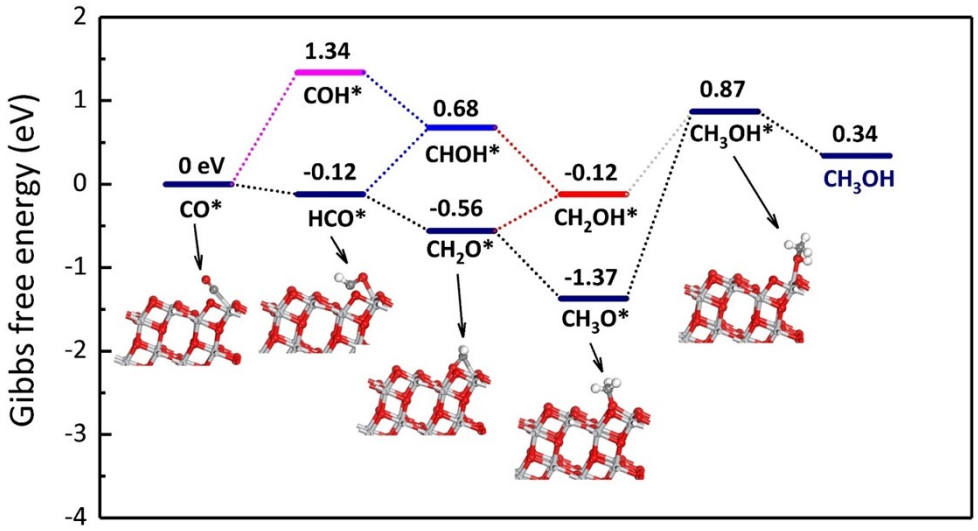

Fig. S17. Free energy diagrams calculated for the pathways of CO reduction to CH_3OH on O-vacancy/TiO_2(101) surfaces (Dark gray: C; light gray: C; red: O; white: H).

Table S1. Zero-point energy (ZPE) and entropy corrections (TS) at T = 298 K for gaseous molecules.

Adsorbate	ZPE (eV)	TS (eV)
H_2	0.28	0.40
H_2O	0.57	0.58
CO	0.14	0.61
CH_4	1.19	0.58
CH_3OH	1.36	0.74
CH_3CH_2OH	2.11	0.82
CH_3CHO	1.47	0.57
CH_3COCH_3	2.21	0.68

Table S2. The adsorption energies [a], Zero-point energy (ZPE, in eV) and entropy correction (TS, in eV) at T = 298 K. All values are given in eV.

Adsorbate	O-vacancy/TiO_2(101)			TiO_2(101)		
	Adsorption energy (eV)	ZPE (eV)	TS (eV)	Adsorption energy (eV)	ZPE (eV)	TS (eV)
*CH_3OH	–1.21	1.44	0.22	–0.66	1.39	0.36
*CH_3O	–4.02	1.11	0.14	–2.06	1.03	0.05
*CH_2O	–1.69	0.79	0.13	–1.32	0.86	0.11
*CHO	–2.76	0.47	0.14	–2.81	0.56	0.10
*CO	–0.86	0.18	0.20	–0.42	0.18	0.21
*H_2O	–1.40	0.66	0.09	–1.03	0.67	0.13
*OH	–4.72	0.37	0.07	–1.16	0.32	0.14
*COCO	–2.37	0.43	0.29			
*COC	–8.34	0.35	0.19			
*COCH	–3.62	0.62	0.24			
*$COCH_2$	–0.96	0.91	0.17			
*$COCH_3$	–2.49	1.22	0.25			
*$COCOCH_3$	–3.15	1.47	0.34			
*$COHCOCH_3$	–4.30	1.79	0.34			
*$CCOCH_3$	–4.29	1.35	0.25			
*$CHCOCH_3$	–4.77	1.65	0.26			
*CH_2COCH_3	–4.08	1.97	0.24			
*CH_3COCH_3	–1.30	2.26	0.44			
*COCOH	–3.00	0.74	0.27			
*COCHO	–3.03	0.74	0.18			
*COCHOH	–3.53	1.05	0.20			
*$COCH_2OH$	–3.08	1.37	0.22			
*$COHCH_2OH$	–3.38	1.68	0.23			
*$HCOCH_2OH$	–2.14	1.68	0.26			
*$CHOHCH_2OH$	–2.67	1.95	0.27			
*CH_2OHCH_2OH	–2.86	2.34	0.26			
*$CHCH_2OH$	–4.09	1.59	0.17			
*CH_2CH_2OH	–3.05	1.86	0.20			
*CH_3CH_2OH	–1.34	2.19	0.26			
*CH_3CHOH	–1.93	1.78	0.31			
*CH_3CHO	–1.22	1.51	0.35			
*CH_2OH	–2.47	1.18	0.13			
*CHOH	–2.73	0.78	0.16			
*COH	–2.94	0.48	0.04			

[a] The adsorption energy is defined as $E_{ad} = E_{slab+A} - E_{slab} - E_A$, where the E_{slab+A} is the total energy of the slab with adsorbate, E_{slab} is the energy of surface, and E_A is the energy of gas-phase adsorbate A.

Table S3. Control experimental results of POM over the blank RGO and RGT90 catalysts.

entry	Reactant	oxidant	Catalyst	Temperature (°C)	Light Source	Product
1	10%CH_4/Ar	H_20(g)	RGO	60	hv	None
2	Ar	H_20(g)	RGT90	60	hv	H_2
3	10%CH_4/Ar	None	RGT90	60	hv	None
4	10%CH_4/Ar	H_20(g)	None	60	hv	None
5	10%CH_4/Ar	H_20(g)	RGT90	60	None	None
6	10%CH_4/Ar	H_20(g)	RGT90	60	hv	H_2 and oxygenates

Table S4. Yield comparison of all products (including trace C_2H_6 and C_2H_4) over T20 and RGTX for POM with H_2O under simulated sunlight irradiation.

Catalyst	Yield ($\mu mol \cdot g_{cat}^{-1} \cdot h^{-1}$)							
	C_2H_6	C_2H_4	CO	Methanol	Aldehyde	Ethanol	Propanal	Acetone
T20	0.19	0.18	19.75	12.86	24.00	1.64	3.71	9.07
RGT20	0.25	0.23	16.19	10.02	33.11	2.46	2.04	15.91
RGT30	0.34	0.30	11.42	9.43	37.93	6.03	7.38	16.81
RGT40	0.63	0.17	15.70	8.91	50.91	7.99	10.38	22.84
RGT50	0.64	0.20	19.04	7.66	80.04	10.47	7.59	58.52
RGT60	0.68	0.63	21.32	9.72	117.29	18.40	22.47	69.52
RGT70	0.95	0.50	24.27	9.57	141.43	35.21	18.64	73.14
RGT80	1.02	0.78	22.82	8.25	209.46	13.29	27.57	114.96
RGT90	1.23	0.94	27.32	12.96	289.61	32.46	45.54	191.25

Table S5. Free energaies of the elementary steps involved in CO formation through photooxidation of CH_3OH by •OH radicals on TiO_2(101) surfaces and O-vacancy/TiO_2(101) surfaces.

Elementary steps	ΔG (eV)	
	TiO_2(101)	O-vacancy/TiO_2(101)
$CH_3OH^*+\cdot OH \rightarrow CH_3O^*+H_2O$	0.18	0.26
$CH_3O^*+\cdot OH \rightarrow CH_2O^*+H_2O$	–1.72	0.81
$CH_2O^*+\cdot OH \rightarrow CHO^*+H_2O$	–0.22	0.14
$CHO^*+\cdot OH \rightarrow CO^*+H_2O$	0.52	0.12

Table S6. Free energies of the elementary steps involved in CH_3CH_2OH and CH_3CHO generation from CO reduction on the O-vacancy/TiO_2(101) surface.

Elementary steps	ΔG (eV)
$2CO^* \rightarrow COCO^* + *$ (non-electrochemical)	0.34
$COCO^* + H^+ + e^- \rightarrow COCOH^*$	–0.09
$COCO^* + H^+ + e^- \rightarrow HCOCO^*$	–0.84
$COCOH^* + H^+ + e^- \rightarrow COCHOH^*$	–0.56
$HCOCO^* + H^+ + e^- \rightarrow COCHOH^*$	0.19
$COCHOH^* + H^+ + e^- \rightarrow COCH_2OH^*$	–0.27
$COCH_2OH^* + H^+ + e^- \rightarrow CHOCH_2OH^*$	–0.43
$COCH_2OH^* + H^+ + e^- \rightarrow COHCH_2OH^*$	0.63
$CHOCH_2OH^* + H^+ + e^- \rightarrow CHOHCH_2OH^*$	0.75
$COHCH_2OH^* + H^+ + e^- \rightarrow CHOHCH_2OH^*$	–0.32
$CHOHCH_2OH^* + H^+ + e^- \rightarrow CHCH_2OH^* + H_2O(g)$	0.41
$CHCH_2OH^* + H^+ + e^- \rightarrow CH_2CH_2OH^*$	–1.14
$CH_2CH_2OH^* + H^+ + e^- \rightarrow CH_3CH_2OH^*$	–0.93
$CH_3CH_2OH^* \rightarrow CH_3CH_2OH(g) + *$ (non-electrochemical)	1.34
$CH_3CH_2OH^* \rightarrow H^+ + e^- + CH_3CHOH^*$	1.28
$CH_3CHOH^* \rightarrow H^+ + e^- + CH_3CHO^*$	–1.05
$CH_3CHO^* \rightarrow CH_3CHO(g) + *$ (non-electrochemical)	1.22

Table S7. Free energies of the elementary steps involved in CH_3COCH_3 generation from CO reduction on the O-vacancy/TiO_2(101) surface.

Elementary steps	ΔG (eV) (0V)
$2CO^* \rightarrow COCO^* + *$ (non-electrochemical)	0.34
$COCO^* + H^+ + e^- \rightarrow COCOH^*$	–0.09
$COCOH^* + H^+ + e^- \rightarrow COC^* + H_2O(g)$	–0.48
$COC^* + H^+ + e^- \rightarrow COCH^*$	–0.67
$COCH^* + H^+ + e^- \rightarrow COCH_2^*$	–0.79
$COCH_2^* + H^+ + e^- \rightarrow COCH_3^*$	–0.89
$COCH_3^* + CO^* \rightarrow COCOCH_3^* + *$ (non-electrochemical)	–0.38
$COCOCH_3^* + H^+ + e^- \rightarrow COHCOCH_3^*$	0.30
$COHCOCH_3^* + H^+ + e^- \rightarrow CCOCH_3^* + H_2O(aq)$	1.02
$CCOCH_3^* + H^+ + e^- \rightarrow CHCOCH_3^*$	–1.32
$CHCOCH_3^* + H^+ + e^- \rightarrow CH_2COCH_3^*$	–1.08
$CH_2COCH_3^* + H^+ + e^- \rightarrow CH_3COCH_3^*$	–0.13
$CH_3COCH_3^* \rightarrow CH_3COCH_3(g) + *$ (non-electrochemical)	1.30

Table S8. Free energies of the elementary steps involved in CH_3OH generation from CO reduction on the O-vacancy/TiO_2(101) surface.

Elementary steps	ΔG (eV)
$CO^* + H^+ + e^- \rightarrow CHO^*$	–0.12
$CO^* + H^+ + e^- \rightarrow COH^*$	1.34
$CHO^* + H^+ + e^- \rightarrow CH_2O^*$	–0.44
$CH_2O^* + H^+ + e^- \rightarrow CH_3O^*$	–0.81
$CH_3O^* + H^+ + e^- \rightarrow CH_3OH^*$	0.50
$CH_2O^* + H^+ + e^- \rightarrow CH_2OH^*$	0.44
$CH_2OH^* + H^+ + e^- \rightarrow CH_3OH^*$	–0.75
$CHO^* + H^+ + e^- \rightarrow CHOH^*$	0.80
$COH^* + H^+ + e^- \rightarrow CHOH^*$	–0.66
$CHOH^* + H^+ + e^- \rightarrow CH_2OH^*$	–0.80